Journal of Electric Propulsion

RESEARCH Open Access

Design of a power processing unit with integrated telemetry for a vacuum arc thruster as part of the SeRANIS mission

Roman Forster[1*], Michal Szulc[2] and Jochen Schein[3]

*Correspondence:
Roman Forster
roman.forster@unibw.de
[1]Institute of Physics, University of the Bundeswehr Munich, Neubiberg (Munich), Germany
[2]Institute of Automation and Control, University of the Bundeswehr Munich, Neubiberg (Munich), Germany
[3]Institute of Physics, University of the Bundeswehr Munich, Neubiberg (Munich), Germany

Abstract

In this work the design and development of a power processing unit for a vacuum arc thruster is presented. The thruster is part of the Seamless Radio Access Networks for Internet of Space (SeRANIS) mission of the University of the Bundeswehr Munich, which will work as first multifunctional laboratory in orbit with public access. In addition to the basic functionality of generating a voltage peak for igniting the thruster, the power processing unit is equipped with techniques for controlling the ignition sequence and monitoring desired key values. The ignition procedure starts with generating the first trigger signal up to the point where a full-blown plasma is established. The PPU guarantees reliable performance by blocking every additional incoming signal while the ignition sequence is under way and the separation of the satellite's power bus before the thruster discharges. The status of the power processing unit is constantly controlled and information is provided whether ignition was successful or not. The functionality of this circuit is based on simulation before assembly and testing. In addition, the presented system was designed to pass a test cycle of mechanical, thermal and electrical tests before being declared ready for the space mission.

Introduction

The number of successful launches of small satellite missions has increased immensely in recent years. Nanosatellites, particularly the so-called CubeSats, are becoming more and more popular. Due to their miniaturization and standardization, the costs of launching CubeSats has been reduced significantly, making them more attainable for start-ups and research institutes [1–4]. One challenge that needs to be overcome with nanosatellites is their positioning with a suitable propulsion system. Due to mass and size limitations, small and lightweight systems are in demand. Apart from these limitations, the envisaged propulsion system must enable precise attitude control of the satellite. This is desirable, among other things, because the CubeSats are often intended to be deployed as communicating swarms [5–7]. The vacuum arc thruster (VAT) has proven to be a suitable electric propulsion system for this application and has already been tested in

few space missions [8–10]. The thrust in a VAT is generated by a highly ionized and energetic metallic plasma jet that occurs after a discharge between the electrodes. To be more precise, the plasma jet is created by the so-called cathode spots, i.e. points where the arc converts cathode material into a plasma [11]. The vacuum arc thruster has many advantages. One of the biggest advantages is its simplicity, as the system does not require a gaseous propellant and therefore does not require a complex and space-consuming supply system. Instead, the cathode material serves as propellant for the vacuum arc thruster. Furthermore, the system can be easily scaled up. These two properties in particular make this electric propulsion system attractive for nanosatellites [12, 13]. In 2016, the μCAT of the Micropropulsion and Nanotechnology Laboratory from the George Washington University was tested on the BRICSat-P satellite [8]. In 2018, the CANYVAL-X nanosatellite, which was a collaboration between NASA, Korea Aerospace Research Institute and Korea's Yonsei University, was launched with the aforementioned μCAT [14]. Another nanosatellite equipped with a VAT system was the HORYU-4 developed by the Kyushu Institute of Technology, which also started its mission in 2016. The onboard VAT was used for attitude control, orbital station keeping or as momentum wheels [10]. In addition to these realized missions, numerous theoretical considerations describing the VAT as a suitable electric propulsion system for nanosatellite missions can be found [15–17]. Research to date has focused mainly on the development and optimization of the thruster head or parts of the power processing unit (PPU) that influence the operating point of the thruster head [18–22]. There are also attempts to integrate such an electric propulsion system into small satellites [23, 24]. A description of a control system using vacuum arc thrusters with a dedicated power supply for a pico-satellite can be found in [25]. Some systems are commercially available and have an open license, i.e. the description of their PPU circuits is available for download [26]. However, if the system is controlled by a microcontroller, detailed information about the exact operating principle of the PPU is usually missing. The approach chosen by the authors in this paper is to keep the description of the PPU and especially the integrated telemetry as transparent as possible.

To make this electric propulsion system more attractive for future satellite missions, VAT systems have been additionally tested and optimized in regard to the operating lifetime to extend the possible mission duration [27, 28]. Participation in SeRANIS project offers an exceptional opportunity to test one of the developed VAT systems under in-space conditions. The satellite developed in the SeRANIS project, called Athene 1, can be seen as a multi-functional experimental laboratory operated on LEO in which the VAT is one of many experiments. Further experiments in this mission include space communication, radio science, high-level AI-based autonomy, GNSS technologies, optical & IR Earth Observation, payload operation concepts, modern structures and innovative system-health-monitoring techniques [29, 30]. The mission architecture is explained in detail in [31, 32]. Testing under in-space conditions requires a monitoring system to determine the status, behavior and performance of the thruster on orbit. The obtained data can be then used to improve models and predict the behavior of forthcoming thrusters. Thus, this work describes the detailed design of the power processing unit with corresponding thruster as well as the telemetry required to supply and control the VAT on the Athene 1 satellite.

Materials and methods

In the first section, the VAT and according PPU requirements are described. After that, the mechanical design of the thruster used is shown and explained. Next, the power processing unit for igniting the VAT is described. The pulse timing and the on-board diagnostic circuitry are then explained in detail.

VAT and PPU mission requirements

The supply voltage for the VAT experiment provided by the SeRANIS satellite is unregulated with values ranging between 26 and 32.8 V. The peak input power is limited to 84 W. Based on the input, the PPU should reliably trigger the VAT and provide information about the voltage and current for each pulse. The operating lifetime of the VAT achieved under laboratory conditions reached over 10^7 pulses [27]. Thus, for in-space conditions the VAT is set to achieve at least 10^5 pulses. A study of the thrust and operating lifetime of the thruster in combination with the proposed PPU is beyond the scope of this paper and will be presented in a future manuscript.

Mechanical design of the vacuum arc thruster

The presented VAT consists of two cylindrical electrodes, which are separated by a cylindrical insulator. Both electrodes, the anode made of stainless steel and the cathode made of titanium, are arranged concentrically. The thruster head and an exploded view of it can be seen in Fig. 1.

The two holders used for positioning and insulating are made of polyether ether ketone (PEEK). The insulator fits tightly into the anode. The cathode, in turn, is inserted into the insulator. The anode is mounted to the large PEEK holder via three M2×10 screws from the back side of the assembly. The larger PEEK holder is designed to hold the cathode and to provide a perfect fit of the insulator. The cathode is contacted by an aluminum ring that slides onto it. This ring is attached to the cathode with three M1.6 grub screws. The shaft of the second and smaller PEEK holder fits exactly into the inner diameter of the cathode and is screwed via the larger PEEK holder to the anode. This guarantees a tight fit of all components. The electrodes are contacted through ring terminals, the cathode terminal is screwed to the aluminum ring, as shown in Fig. 1, and the anode terminal is attached with one of the screws holding the smaller PEEK holder.

The VAT head described above is packaged with the complete electronic circuit in an aluminum chassis, as shown in Fig. 2. The thruster head itself is mounted to the top plate of the aluminum chassis via three M2×10 screws, with the outlet of the VAT pointing away from the chassis. The PEEK holder guarantees electrical isolation between

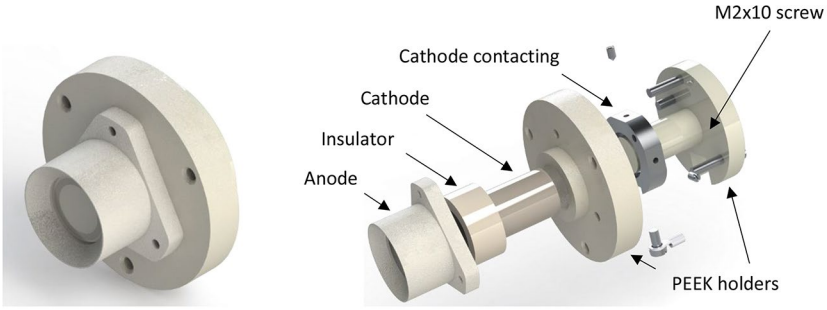

Fig. 1 Thruster head of the VAT; Left: Total view; Right: Exploded view

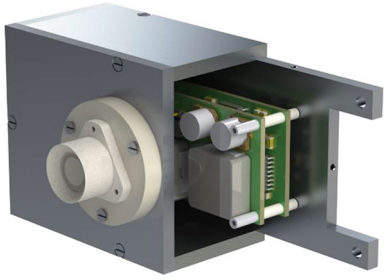

Fig. 2 VAT with aluminum chassis for the power processing unit as sectional view

electrodes and chassis. The chassis is attached to the satellite with four M4×10 screws. The housing has a size of 98 mm x 58 mm x 39 mm, in which the PPU is located. For shielding purposes, the wall thickness of the housing is four millimeters. An electrical connector is integrated on the back plate of the chassis. The total height, measured from the connector on the back plate to the top of the VAT head, is 65 mm.

Operating mode of the vacuum arc thruster

The thruster described above is designed to operate in the so-called triggerless mode. In this operating mode, the breakdown voltage is reduced due to a conductive path on the insulator between the two electrodes. Initially the insulator is coated with a thin layer of graphite. When the thruster is triggered, current flows across this thin conductive layer and destroys it due to Joule heating. However, due to this conductive layer, which essentially decreases the A-C gap, the breakdown voltage is reduced and a discharge pulse is initiated which creates a plasma jet from the cathode material. Part of this metal plasma is redeposited on the surface of the insulator. As a consequence, the conductive layer is restored. In an ideal world, the renewal of the layer would exactly counteract the earlier erosion, but this is not the case hence triggerless operation is reliably only for a certain number of pulses and is the main limiting factor for the operating time of a VAT. After -design and performance dependent -several thousand to several hundred thousand discharge pulses, the layer may become either too conductive due to increased deposition or the gap between the electrodes becomes too large due limited re-deposition combined with erosion of the cathode. Nonetheless, when carefully selecting operational parameters in combinations with a suitable mechanical design, the thruster can be operated at lower ignition voltages (than when using a non-triggerless mode) for an extended period, while the conductive path is constantly renewed [33, 34]. Furthermore, no additional features such as separate trigger electrodes or a high-voltage ignition circuit are required.

Power processing unit

In order for the thruster to ignite, a suitable power processing unit is required. The PPU used in this work is based on the principle of an inductive energy storage (IES). The IES principle has been widely used in research and its advantages such as simplicity, robustness, and low mass have been highlighted on many occasions [18–20, 35]. It ensures a sufficiently high voltage peak for the breakdown between anode and cathode, when operating in the triggerless mode. The exact design of the PPU is explained in the following.

Inductive energy storage

A schematic of the IES highlighting the main components is displayed in Fig. 3. A storage inductor with an inductance of 150 µH was chosen. To charge the inductor, an insulated gate bipolar transistor (IGBT) with a high collector-to-emitter voltage is triggered. After the charging time is completed, the IGBT opens and the inductor induces a voltage peak of $L * \frac{dI}{dt}$.This voltage peak ignites the plasma. After ignition, the energy stored in the inductor and in a capacitor connected in parallel to the thruster supports the discharge. The capacitor therefore serves as a primary energy source and in this case has a capacity of 220 µF.

The principle of the developed control and diagnostic circuit is based to large extend on the charging of the above-mentioned 220 µF capacitor. After the capacitor is fully charged, the satellite power bus is disconnected and the thruster is ignited as described. Disconnecting the power bus before each discharge prevents unwanted electrical interferences from being fed back into the supply. The detailed implementation of the circuit is discussed in the following sections.

Telemetry

Four vacuum arc thrusters are planned on the Athene 1 satellite. Every VAT head will be equipped with its own PPU, as described in the previous section, and creates a so-called thruster package. These four thruster packages are then connected to the power supply and control unit (PSCU) that not only supplies and controls the VAT packages, but also communicates with the satellite's control system. The PSCU is connected to the unregulated power bus of the satellite, which provides voltages up to 32 V, and generates from that a constant voltage of 24 V with a maximum current of 3 A to supply the PPUs. The PSCU's microcontroller also processes the satellite commands and controls the PPUs accordingly. The VATs are triggered at a desired frequency as soon as the satellite control system gives permission to start the experiment and data collected in the PPU for each discharge pulse is processed by the PSCU and transmitted to the satellite system. Apart from the supply voltage, trigger signal and diagnostic signals (which will be described in the following), the PSCU powers also the control and on-board diagnostic circuits of the PPUs with a voltage of 5 V (called VCC).

In Fig. 4 the principal arrangement of the PSCU and the four VAT packages can be seen. The aim while developing the circuit with its on-board diagnostics was, to make it as robust as possible and, to monitor the most important parameters in order to determine the wear condition of the thruster. It was decided that the circuit should work as autonomously as possible – the PPU only requires the supply voltages of 5 V and 24 V and a trigger signal per charge. Two signals are returned to the PSCU, one corresponding to the capacitor voltage and one corresponding to the discharge current.

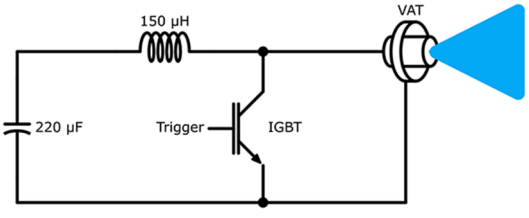

Fig. 3 Principle schematic of an inductive energy storage

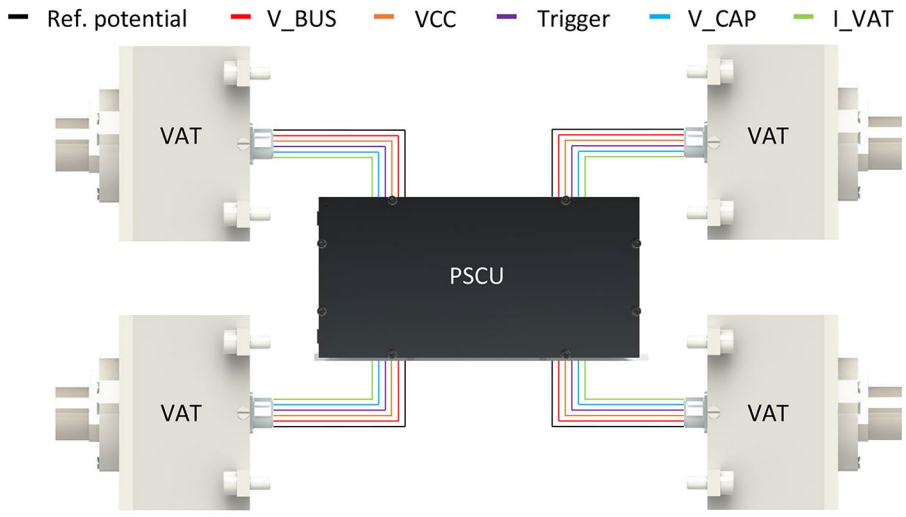

Fig. 4 Principle arrangement of the four thrusters and the PSCU on the satellite

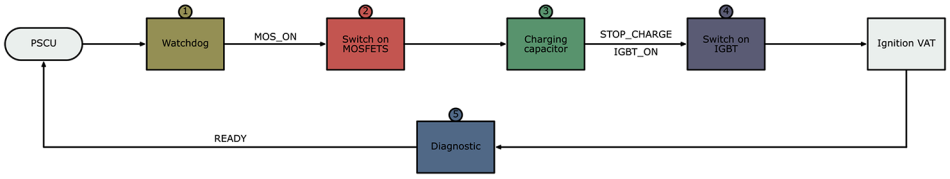

Fig. 5 Rough flowchart with the main components of the circuit and the signal names between the components

Conceptual implementation of the IES for triggerless operation mode

According to the above considerations, the conditions for the implementation of the PPU circuit were determined – the thruster should be driven by an IES and operated in the so-called triggerless mode. To maintain clarity in the following discussion, the developed circuit can be divided into five parts according to their function. From now on, these five parts are marked with different colors, as displayed in Fig. 5.

The first part called Watchdog is responsible for correct operation of the circuit. It controls the switching times of the semiconductors and protects the PPU from unintentional trigger signals by disabling and enabling the trigger input. The second part called MOSFETs controls the power switches respectively their corresponding gate driver, which are responsible for isolating the PPU from the satellite's power bus while a discharge is occurring. The MOSFETs are charging the third part, the capacitor of the IES. This part of the control circuit also provides feedback about the capacitor's charge status – a discharge occurs only when the capacitor is fully charged. The fourth part, into which the circuit can be divided, comprises the IGBT of the IES with a matching gate driver. The last part is the diagnostic of the PPU, which includes current and voltage measurements. Between the parts of the circuit the generated signals with their accorded names are listed in the upper image. These signals are responsible for the correct and ordered ignition sequence All parts are explained in detail in the following sections.

In Fig. 6 the schematic of the integrated IES of the circuit with additional components is shown.

The basic IES with the 220 µF capacitor, 150 µH inductor and IGBT as semiconductor can be recognized easily. Three MOSFETs and an accorded gate driver are added to

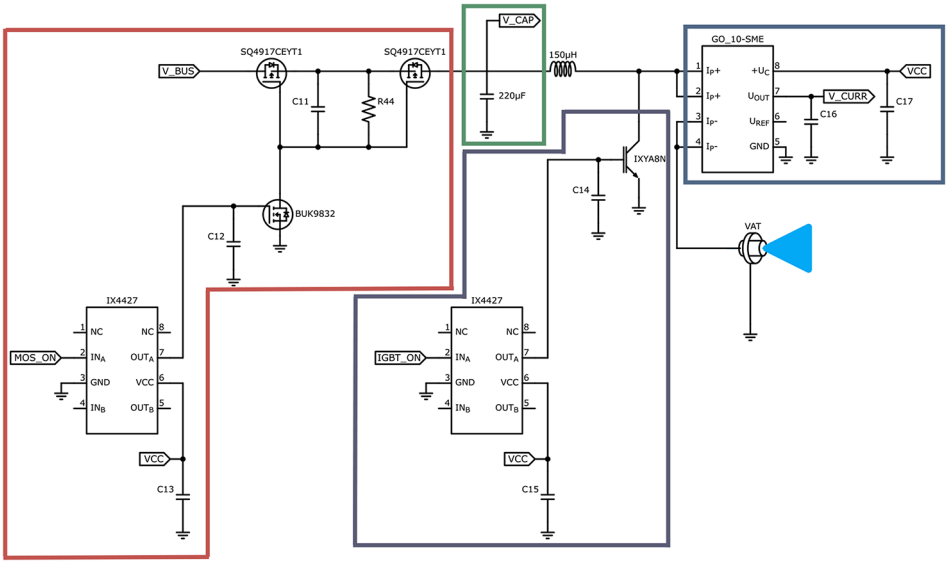

Fig. 6 Realized IES with additional components

connect the power bus of the satellite in case of charging the capacitor and disconnect it in case of igniting the thruster (red box). The IGBT is also equipped with a suitable low side gate driver (purple box). As mentioned above the voltage V_CAP across the capacitor (green box) and the discharge current detected by the GO-10-SME sensor (blue box) are monitored.

The charging of the described IES with subsequent ignition of the thruster is determined by a defined sequence, which enusres a safe and controlled execution of the experiment. This sequence is described in detail in the flowchart below.

At first, the PPU of the VAT has to be supplied by VCC from the PSCU. Then the PSCU has to supply 24 V to the desired VAT, which should be used in the experiment. The thruster is ready for use at this point and can be triggered by the PSCU. An incoming trigger starts the ignition sequence, which is depicted in Fig. 7.

After a trigger is received, the Watchdog part generates a MOS_ON signal. The Watchdog disables the input of the PPU so that the started ignition sequence is not disturbed by further unintended trigger signals, i.e. multiple triggering of the circuit is not possible as long as the ignition sequence has not been successfully completed. The MOS_ON signal is amplified by a low-side gate driver and triggers an n-channel MOSFET, which then switches a pair of two p-channel MOSFETs (see Section physical implementation of the PPU) to charge the capacitor of the IES. As mentioned before, the capacitor serves as the primary energy source. The state of charge of the capacitor is monitored and when fully charged a signal called STOP_CHARGE is generated. The Watchdog receives the STOP_CHARGE signal and turns off the MOSFETs. At the same time, an IGBT_ON signal is generated, which triggers the IGBT to charge the inductance via a low-side gate driver. After a fixed time, the IGBT is switched off, producing the desired voltage peak across the inductor to ignite the VAT. In case of ignition, that means a current flow through the current sensor, a READY signal is generated, which enables the input of the PPU again. The switching times are chosen so that the ready signal can only be generated after a discharge. Accordingly, the trigger input of the PPU is only enabled again after a successful discharge. The integrated on-board diagnostics measures the voltage of the

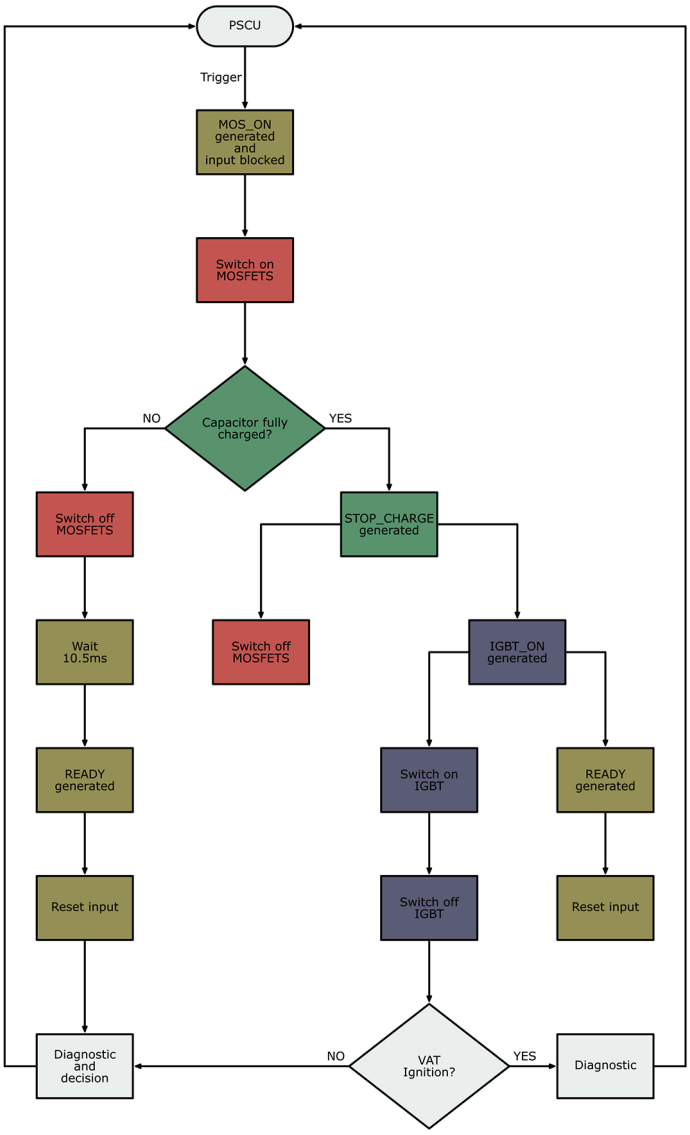

Fig. 7 Flowchart of the ignition sequence of a VAT. The parts of the circuit are colored accordingly

capacitor (called V_CAP) and the discharge current of the thruster. After a discharge, the measured values are evaluated by the PSCU and thus provide information about the respective discharge.

The STOP_CHARGE signal is not generated if there is a malfunction, i.e. if the MOS_ON time is too short to fully charge the capacitor. In such a case, the trigger input of the PPU would remain disabled. In that case, a second timing chip is triggered at trigger input (in parallel to the MOS_ON signal), which generates a READY signal after a fixed time that is much longer than required for the regular ignition sequence. This prevents the input from hanging up and the entire PPU from having to be restarted as a consequence. If a discharge does not occur after a subsequent trigger, the measured values have to be analyzed to determine why the capacitor was not fully charged, and the PPU reboots by switching off both supply voltages.

The monitored parameters are also used by the PSCU to estimate the thruster's operating time. If the end of the service life is not reached, a new trigger pulse can initiate the next ignition sequence.

In general, the end of the thruster's operating time can be reached due to cathode erosion or due to a short circuit between the electrodes. In the first case, the cathode is eroded to such an extent that the voltage peak provided by the PPU is not high enough to ignite a discharge. In the second case, the conductivity of the layer deposited on the insulator is so high that it represents a short circuit between the electrodes for the PPU. These two, as well as other failure cases described below, can be detected with the on-board diagnostics.

The possible combinations of the monitored parameters, i.e. capacitor voltage and discharge current, and their interpretations with possible actions are listed in Table 1. If the voltage V_CAP across the capacitor and the monitored current are unequal to zero, the capacitor was fully charged and a current was flowing over the VAT as listed in the first column. As consequence, an ignition took place and the amount of energy consumed can be estimated in post-processing. This case is considered a correct operation and the pulse counter can be incremented by the PSCU microcontroller.

A non-zero V_CAP and no current flow across the thruster, as shown in the second column of Table 1, indicates a failure in which the thruster did not ignite. This condition can be caused by one of the following malfunctions. Either the capacitor was not fully charged (i.e. the charging current was too low), or the IGBT did not switch off or the thruster is reaching the end of its operating time due to erosion. In the first case, if there is not enough charge stored in the capacitor, no STOP_CHARGE signal is generated and the Watchdog circuit does not trigger the IGBT. As a countermeasure, the frequency of the trigger can be increased (i.e. a pulse train is sent by the PSCU) to achieve the desired amount of energy. If the IGBT does not switch off, the capacitor is short-circuited with the inductance and a voltage pulse necessary for ignition cannot be generated. A countermeasure in this case is to reboot the PPU by switching off both supplies, the power bus and VCC. If the situation persists after a trigger pulse train and a restart of the PPU, then the induced voltage peak is not sufficient to ignite the VAT and, as a result, the end of the thruster's operating time is reached. Such a thruster is then marked accordingly by the PSCU control system and excluded from further experiments.

If an almost zero voltage is measured across the capacitor, but at the same time, a current flows through the VAT, the electrodes are most probably short-circuited. In this case, the thruster reaches its end of life and is excluded from further experiments.

Table 1 Possible failure cases and interpretations

On-board diagnostics	**V_CAP ≠ 0 & I ≠ 0**	**V_CAP ≠ 0 & I = 0**	**V_CAP ~ 0 & I ≠ 0**	**V_CAP = 0 & I = 0**
Result	Ignition	No ignition	No ignition	No ignition
Interpretation	No failure; Correct operation	Possible failure cases: 1. Capacitor not fully charged; 2. IGBT stuck; 3. End of lifetime	Possible failure case: End of lifetime	Possible failure case: No V_BUS
PSCU action	Pulse energy estimation based on V_CAP, Counting of ignitions	1. Send a trigger train; 2. Reboot the PPU; 3. VAT damaged; exclude from further use	VAT damaged; Exclude from further use	Check PSCU or satellite bus

The last possible failure case listed in the fourth column of Table 1 represents the situation where both monitored values are zero. In this error case, no power bus voltage appears to be applied. Therefore, the PSCU or the satellite power bus have to be inspected.

Physical implementation of the PPU

After the supply voltage VCC is applied to the circuit, the trigger input is initialized by a Darlington transistor pair, which is connected to the XOR gate chip CD4070B via the RD3 Signal. The XOR gate generates an initial falling edge that enables the trigger input, thus preparing the PPU circuit for operation.

The ignition sequence starts with an incoming trigger from the microcontroller of the PSCU. For a galvanic separation, the trigger signal is transmitted to a CD4027 dual J-K flip flop via an HCPL-181 optocoupler. The J-K flip flop operates as an R-S type flip flop - the SET input is disabled after receiving a trigger and enabled after receiving a falling edge of the READY signal at the RESET pin when the ignition sequence is completed. This ensures that an unwanted trigger signal is ignored during operation until the READY signal resets the CD4027. The output signal of the flip flop is passed to the first CD4538 dual monostable multivibrator. Part A of the first CD4538 generates the MOS_ON signal with a maximum pulse duration of 10 ms, for which the MOSFETs are switched on. The signal is therefore amplified by an IX4427 low-side gate driver (see Fig. 6) and switches a BUK9832 n-channel MOSFET, which then switches a pair of p-channel MOSFETs (SQ4917CEYT1). These MOSFETs switch the power bus and control the charging of the 220 µF capacitor. A back-to-back connection of transistors ensures a bidirectional protection from unwanted electrical interference back to the 24 V bus. The charging process is monitored by an MC33078 operational amplifier, which compares the voltage across the capacitor (called V_CAP) to a predefined reference value. When the input voltage exceeds the set threshold of 3.9 V, which corresponds to 23.85 V of V_CAP, the STOP_CHARGE signal goes low. The duration of the MOS_ON pulse is chosen so that the capacitor is definitely fully charged during this time. In normal operation, a significantly shorter charging time is required and therefore the first retrigger able multivibrator is usually reset beforehand by a falling edge of the STOP_CHARGE signal. The output signal of the CD4027 is connected as well to a second CD4538 multivibrator. This chip serves as a backup reset of the input flip flop in case of a failure if the capacitor is not fully charged within the time specified by the first CD4538. The delay time of the second multivibrator is chosen to be longer than the maximum duration of the ignition sequence. When this delay has expired, the CD4027 is reset with a 10 µs short RD2 pulse via the XOR gate. When the capacitor is fully charged, the STOP_CHARGE signal is passed to the third CD4538 chip to generate a trigger pulse for the IGBT. The so-called IGBT_ON output pulse is delayed by 100 µs to ensure safe switching off of the MOSFETs and has a duration of 500 µs. An identical gate driver IXN4427 as for the MOSFETs is used to control the IXYA8N IGBT (see Fig. 6). The fourth CD4538, which is triggered by the RESET signal, generates the RD1 signal after 750 µs. The RESET signal indicates, that a discharge current took place. After this time, the discharge of the thruster is finished and the ignition sequence has been successfully completed. As a consequence, the trigger input of the PPU can be activated

again. Thus, the 10 µs short RD1 pulse is passed to the XOR gate CD4070 to generate the READY signal to reset the CD4027 flip flop (see Fig. 8).

As described in the previous section, the voltage across the capacitor and the current flowing through the VAT are monitored to provide feedback on the thruster behavior under various conditions. Both signals are converted to a frequency using an operational amplifier-based voltage-frequency circuits (short VFC), which can be seen in Fig. 9. This allows for the frequency signals to be easily passed to the higher-level system (here the

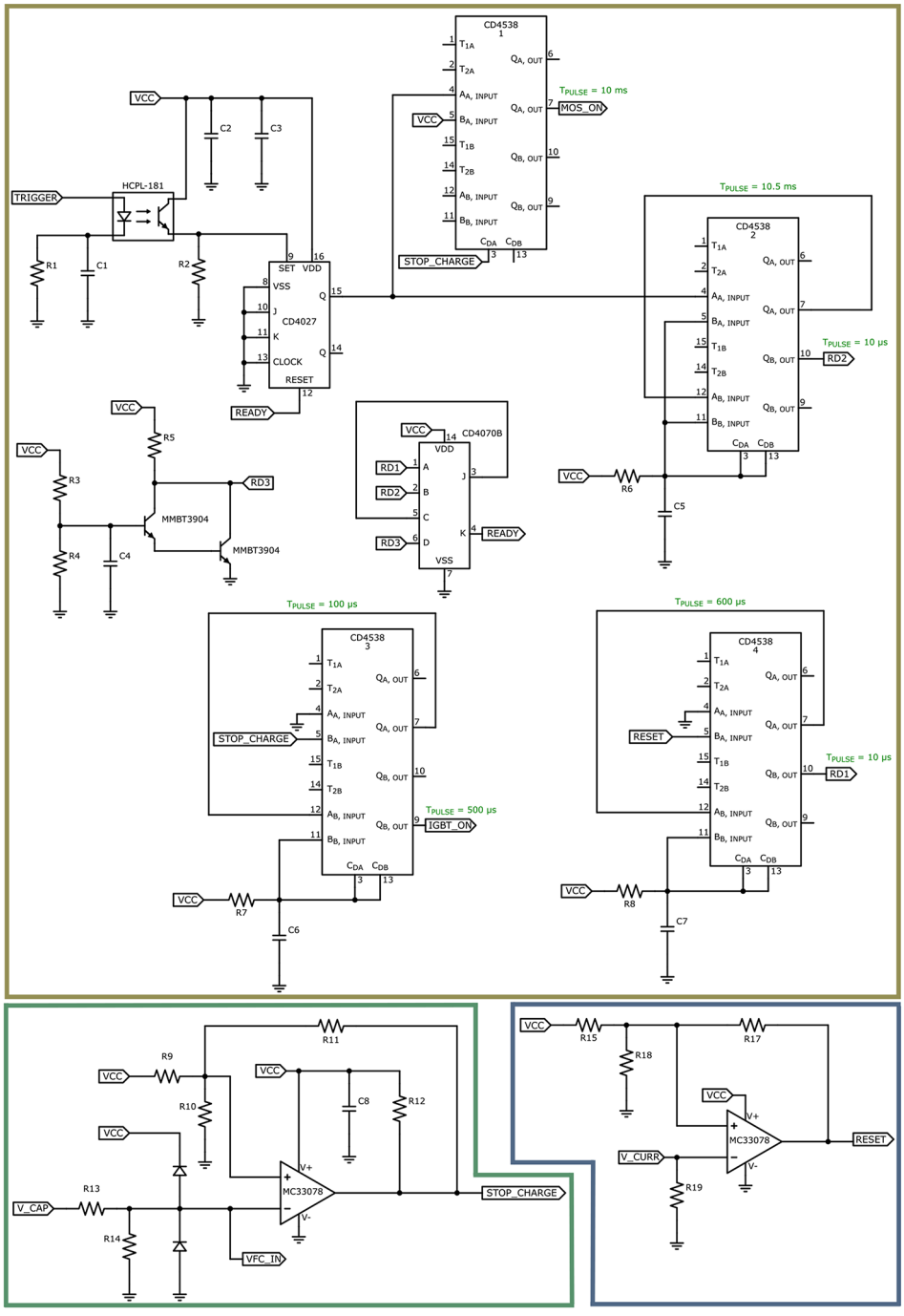

Fig. 8 Control unit of the PPU

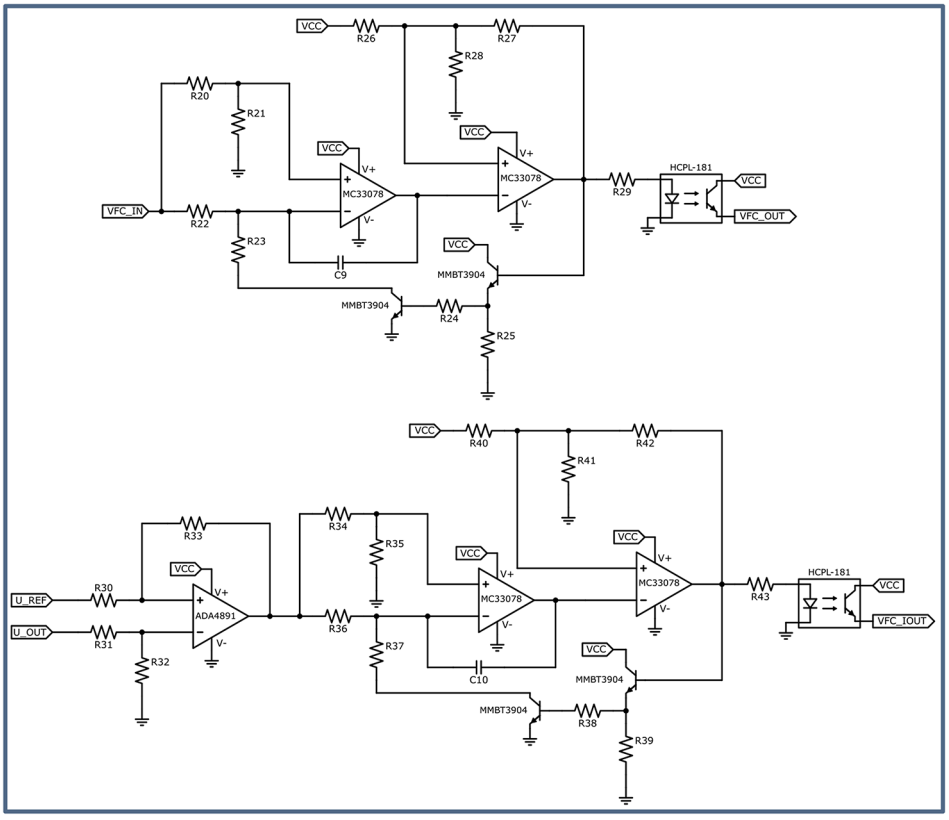

Fig. 9 Diagnostic unit of the PPU

PSCU) with galvanic insulation. In the first case, the voltage V_CAP is directly connected to the converter. The converter puts out a signal with a fixed duty cycle and a frequency ranging between approximately 4.6 kHz and 8.2 kHz, the higher value corresponding to a V_CAP of almost 24 V. For the current measurement, a GO 10-SME current transducer is used. The primary and secondary side of the transducer are galvanically separated and the output signal is referenced to a reference voltage for greater accuracy. Therefore, before the current signal is converted into a variable frequency TTL signal, the first op-amp rescales it to a range of 0 to 5 V. Since the discharge duration is significantly shorter than the charging time of the capacitor (in the range of thirty microseconds), the output frequency of the second VFC has to be increased accordingly. Hence, the output varies between about 800 kHz and 1.3 MHz depending on the discharge current.

In addition to the description above, the following figures show the timing diagrams in order to better clarify the relationships between the signals introduced in Fig. 5. The signals in Fig. 10 correspond to a normal, failure-free ignition sequence.

After VCC is applied and the PPU is initialized, an incoming trigger from the PSCU starts the sequence (denoted with a in Fig. 10). The signal triggers the CD4027 flip flop – the output CD4027_Q goes high. The input of the flip flop then is disabled, any incoming trigger signal is ignored (b) until it is not actively reset by a falling edge of the READY signal. The CD4027_Q triggers a CD4538 multivibrator that generates the MOS_ON signal with a fixed maximum duration of 10 ms. During this time the capacitor is charged. The process can be shortened by the STOP_CHARGE signal when a preset threshold

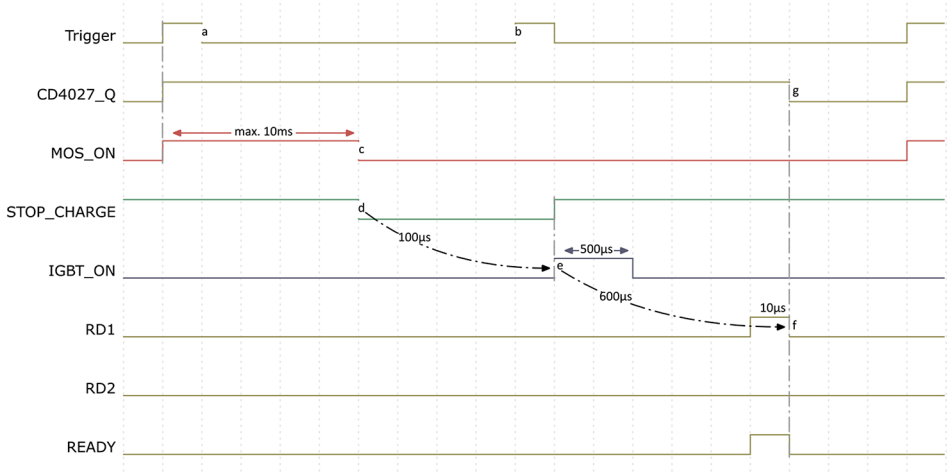

Fig. 10 Timing diagram of the control unit in case of regular operation

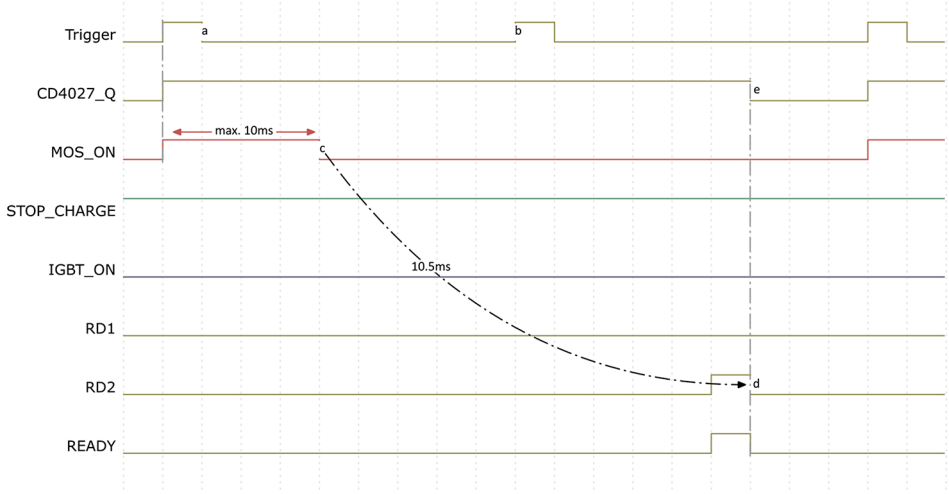

Fig. 11 Timing diagram of the control unit in case of irregular operation

corresponding to a full charge state is reached. Thus, the STOP_CHARGE signal indicates the end of the charging process (c and d). The signal has a negative logic because a falling edge is required to reset the multivibrator. With the MOSFETs switched off, after a short delay of 100 µs, the IGBT_ON signal switches the IGBT on and the inductor is charged for 500 µs (e). Charging the inductor reduces the voltage across the capacitor, resulting in a change in state of the STOP_CHARGE signal. When the IGBT_ON signal goes low, a voltage peak is induced, initiating a discharge of the VAT. The typical discharge duration is in the range of thirty microseconds, so a discharge time window of 250 µs was assumed for the control circuit, taking a safety margin into account. After this time, the RD1 signal is emitted (f), which generates the READY signal via the CD4070 XOR gate. The falling edge of the READY signal resets the CD4027 flip flop (g) and thus a new ignition sequence can be started with the next trigger input.

The timing diagram in Fig. 11 corresponds to an irregular operation mode in which the capacitor is not fully charged.

The ignition sequence begins analogously to the example described above. Now, however, the maximum duration of the MOS_ON signal of 10 ms is not sufficient to fully charge the capacitor. In this case, the threshold for generating the STOP_CHARGE signal is not reached and therefore the IGBT_ON pulse is also not generated. As a result, the thruster does not discharge and the trigger input of the PPU remains disabled (no RD1 signal). To prevent this, a second CD4538 is triggered simultaneously with the output signal from the first CD4538 (as described in previous section), which generates an RD2 signal after a fixed time of 10.5 ms (d). Similarly, to RD1, the RD2 signal generates a READY signal via the XOR gate, thus resetting the input flip flop(e). By doing so, the PPU does not remain permanently blocked after a failed ignition sequence. The charging process can then be started with the next trigger pulse and since the capacitor is pre-charged, the threshold value should be reached this time (as long as there is no other error in the system).

Results

In the first step, the schematic of the PPU explained in the previous section was designed and tested virtually using OrCad Capture 17.4 from the software package made by ©Cadence, San Jose, CA, USA. After this, the circuit was physically assembled and its output behavior was tested.

Simulation

The simulation results of the circuit are displayed in Fig. 12. For the sake of clarity, only one charging cycle of the capacitor is shown. Additionally, the simulated circuit was simplified by replacing the VAT with an ordinary 200 Ω resistor.

Figure 12 shows the charging current (I_CHARGE) and the voltage across the capacitor (V_CAP) as well as the discharge current (I_VAT) and the corresponding voltage (V_VAT). Furthermore, two areas are highlighted in color: the MOS_ON time, during

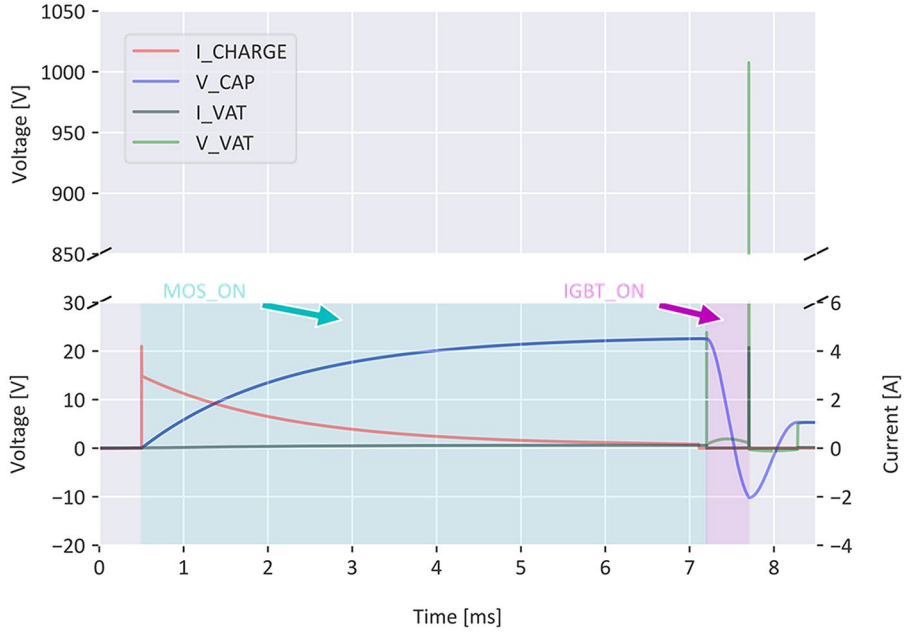

Fig. 12 Simulated charging and discharging of the PPU

which the capacitor is charged, in turquoise, and the IGBT_ON time, which is responsible for generating the peak voltage required to ignite the VAT, in purple. The V_CAP and I_CHARGE curves display the typical charging behavior of a capacitor. If the charging current is limited to 3 A, the charging time lasts about 6.6 ms. Then, the IGBT_ON signal with a pulse width of 500 µs discharges the capacitor through the inductor. The voltage of the capacitor oscillates due to the resonant circuit of the IES. At the moment the IGBT switches off, a voltage peak of up to 1.02 kV is induced by the inductor, which ignites the VAT. The simulated ignition sequence is finished within 7.2 ms. In summary, the simulation results shown in Fig. 12 indicate that the designed PPU circuit works as planned. Therefore, physical assembly of the circuit was done.

Assembled circuit

The following equipment was used to analyze the assembled circuit. The circuit was powered by two HAMEG HM7042-5 electronic power supplies, manufactured by Rohde & Schwarz, Munich, Germany. An LXI G5100A waveform generator, manufactured by Picotest, Phoenix, AZ, USA, was responsible for triggering the PPU input. The voltages were acquired using RT-ZP03 passive probes from Rohde & Schwarz as well as a PPE6kV-A high-voltage passive probe, while currents were acquired using a CP031A and a CP150 probes from Teledyne LeCroy, Chestnut Ridge, NY, USA. The above probes were connected to an HDO 8108 A oscilloscope, also manufactured by Teledyne LeCroy. All relevant data plotted below was recorded by the oscilloscope.

Analogous to Fig. 12, the measured charging and discharging curves of the physical circuit are shown in Fig. 13. The schematic of the physical circuit corresponds to that shown in Fig. 6. In the assembled circuit, the charging of the capacitor lasts about 8.8 ms before the STOP_CHARGE signal indicates the end of charging. The maximum charging current was limited to 3 A, which complies with the current provided by the satellite's power bus. As in the simulation, the IGBT is turned on after MOS_ON ends, and

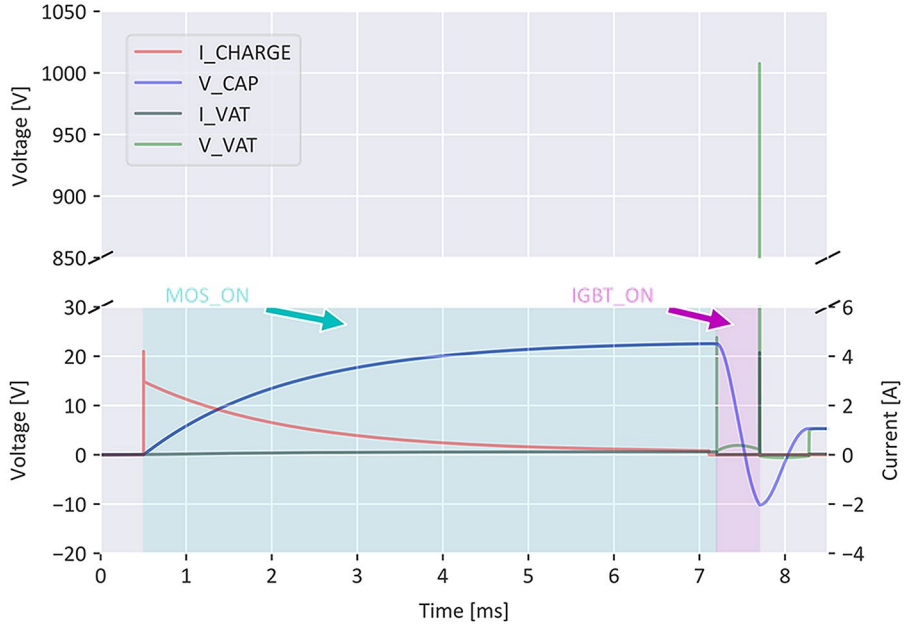

Fig. 13 Experimental charging and discharging of the PPU

enables the ignition of the thruster after turning off. According to the measurement, an induced voltage peak of over 700 V is sufficient to initiate the discharge. During the initial breakdown, a peak current of up to 9.5 A flows across the thruster's electrodes. In order to discuss the discharge behavior of the thruster, the voltage between the electrodes and the current during the discharge are displayed in Fig. 14. The curves in Fig. 14 are averages calculated for 100 discharges and the corresponding deviations are plotted as shaded bands.

Due to the triggerless operation mode of the VAT the initial breakdown between cathode and anode occurs at voltages lower than 500 V, leading to a mean peak current of about 8 A. Then, the current peak decreases rapidly and the discharge ends after about 25 µs. The VAT operates in this mode repeatedly, with a deviation band of about 10% on average. At the beginning and at the end of the discharge the curves show noise due to the ignition and cancellation of the vacuum arc.

Similarly to the charging and discharging comparison between the simulation and experiment, the functionality of parameter monitoring was also tested. For this, the VFC_OUT signal (compare Fig. 9) was calculated and plotted in Fig. 15 with the according voltage V_CAP across the capacitor while charging the PPU.

As the red curve indicates, the capacitor voltage V_CAP is converted into a frequency dependent voltage signal with a fixed duty cycle, as described in the previous section. The frequency ranges between 4.3 kHz and 7.9 kHz, which correspond to approximately 12 V and 24 V respectively. When the capacitor is fully charged, a frequency of about 7.9 kHz is measured. As can be seen in Fig. 15, the designed VFC converter works as planned.

Again, analogous to the simulation presented in Fig. 15, the measured curve of the monitored voltage across the capacitor with according frequency-dependent signal is displayed in Fig. 16.

As depicted in Fig. 16 above, the measured signals are in good accordance with the simulated results. The color scheme is identical to Fig. 15. The lowest voltage value, which can be resolved by the converter is 11.5 V. This corresponds to a frequency of 4.6 kHz. The highest frequency of 8.2 kHz generated on the output of the converter

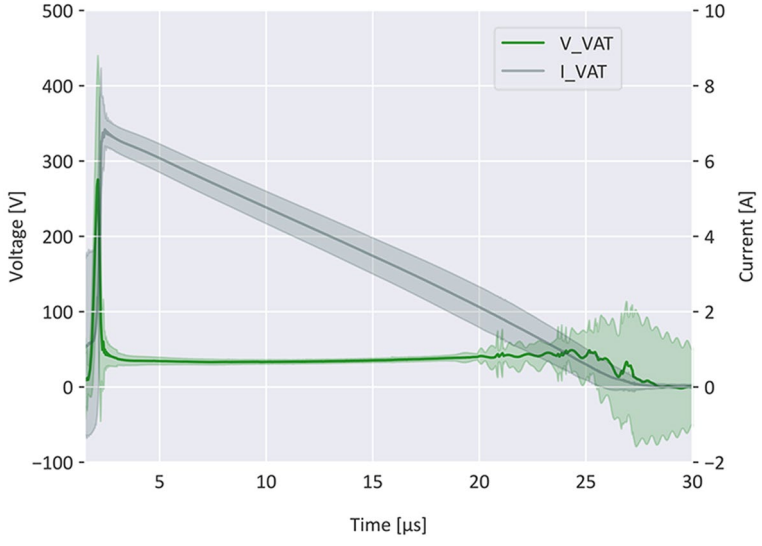

Fig. 14 Mean curves of 100 experimental discharges of the VAT with shaded error bands

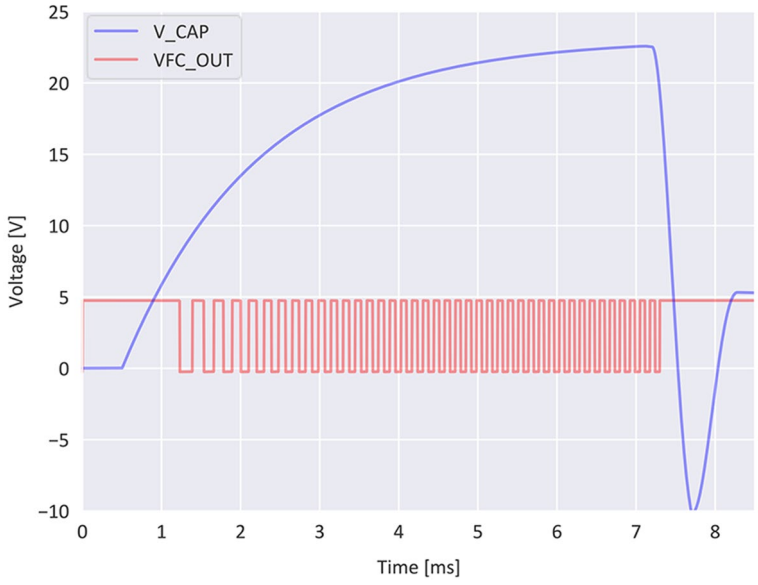

Fig. 15 Simulated monitoring of the parameters

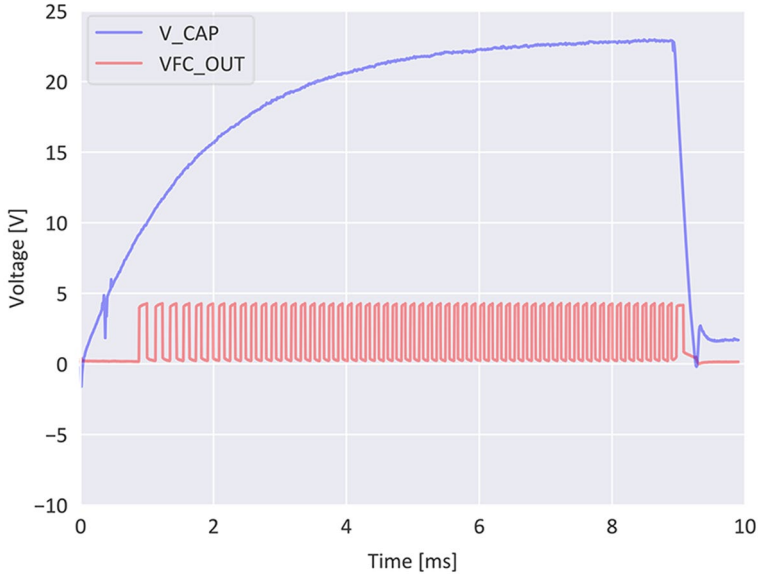

Fig. 16 Results of the monitored parameters of the circuit

indicates the fully charged state of the capacitor and corresponds to a voltage of about 23.5 V.

As shown in Fig. 9, a comparable circuit was used for the monitoring of the discharge current. However, due to the short discharge time of the VAT, the frequency of the output signal has to be significantly higher than that of the V_CAP converter. Additionally, the output signal of the current sensor has to be rescaled with a conversion factor according to the datasheet of the sensor. This leads to output frequencies between 800 kHz and 1.3 MHz, which correspond to a discharge current in the range of 1 A to 13 A.

Conclusion

This work describes the development and functionality of a power processing unit with integrated telemetry for a vacuum arc thruster. The presented PPU with matching VAT are part of the Athene 1 satellite, which is being developed in the SeRANIS mission, and the system is to be flight-approved in accordance with the mission's requirements.

The PPU is based on an inductive energy storage design and includes control and monitoring circuits of the experiment. A watchdog is responsible for the correct and controlled process of charging the capacitor as well as initiating of the discharge. The proposed design proved to be robust, with precautions taken against possible external interference during operation. This includes separating of the PPU from the supplying PSCU and consequently from the power bus of the satellite before the VAT ignites. By doing so, the satellite is protected from possible failure during ignition. In addition, key parameters of the PPU are monitored, processed and sent to the PSCU for downlinking. These are: the voltage across the capacitor and the discharge current flowing across the electrodes of the VAT.

The basic functionality of the circuit was tested virtually and then compared to measurements of a physically assembled circuit with a thruster. The measured charging process of the unit agrees well with the simulation results. The discharge voltage and current curves cannot be directly compared due to simplifications made during simulation of the circuit. However, when comparing the output of the monitored values, both results are again in good accordance. The monitoring of relevant values allows to determine the status of the thruster and detect whether an ignition has occurred or not. It also allows the higher-level system (here the PSCU) to count the number of ignitions and thus assess the operating time of the thruster. Furthermore, the performance of the VAT can be estimated based on the energy consumed per pulse. In case of a failure, the measured values can be used to isolate the fault cause and possible measures can be initiated by the higher-level system.

The control and telemetry part of the PPU circuit operates with a voltage of 5 V, whereas the high-power part of the circuit operates with 24 V. Since the former part consumes a current in the range of tens of milliamperes and the input current of the power part is limited to 3 A, the maximal power consumption of the PPU does not exceed 72 W, which is well within the power budget provided by the satellite. Thus, the electrical requirements of the platform are fulfilled. In addition, the designed telemetry enables to determine the status and the performance of the experiment, and hence meets the requirements set internally for the experiment. The evaluation of the performance and lifetime of the VAT will be presented in a further work.

The circuit used in this work is a laboratory engineering model. The final layout of flight-model needs to be miniaturized and adjusted, as it has to pass system tests. This process will include steps to minimize the influence of EMI, which can be observed in Fig. 14, to prevent any performance disturbances of the internal telemetry as well as other components mounted on the satellite. After these adjustments, the developed package has to pass the mentioned cycle of mechanical, thermal and electrical tests. Mechanically, the VAT package has to withstand a shake and vibration test. During the thermal tests, the system has to operate flawlessly under the most unfavorable hot and cold conditions. The electrical testing focuses on electromagnetic interference measurements that will have to be passed. After each test procedure, the full functionality of the

experiment has to be proven. If all tests are passed, the proposed VAT package is considered approved for flight, can be manufactured and mounted on the Athene-1 satellite.

Acknowledgements
We acknowledge financial support by Universität der Bundeswehr München.

Author contributions
Roman Forster: Writing – review & editing, Writing – original draft, Software, Methodology, Investigation, Formal analysis, Datacuration, Conceptualization. Michal Szulc: Writing – review & editing, Methodology, Investigation, Conceptualization. Jochen Schein: Writing- review & editing, Supervision, Funding, acquisition, Conceptualization.

Funding
This work was supported by SeRANIS (dtec.bw).
Open Access funding enabled and organized by Projekt DEAL.

Data availability
No datasets were generated or analysed during the current study.

Declarations

Competing interests
The authors declare no competing interests.

Received: 29 February 2024 / Accepted: 18 June 2024
Published online: 02 July 2024

References

1. Levchenko I, Bazaka K, Ding Y, Raitses Y, Mazouffre S, Henning T, Klar PJ, Shinohara S, Schein J, Garrigues L et al (2018) Space micropropulsion systems for Cubesats and small satellites: from proximate targets to furthermost frontiers. Appl Phys Reviews 5. https://doi.org/10.1063/1.5007734
2. Lemmer K (2017) Propulsion for CubeSats. Acta Astronaut 134:231–243. https://doi.org/10.1016/j.actaastro.2017.01.048
3. Levchenko I, Xu S, Teel G, Mariotti D, Walker MLR, Keidar M (2018) Recent progress and perspectives of space electric propulsion systems based on smart nanomaterials. Nat Commun 9:879. https://doi.org/10.1038/s41467-017-02269-7
4. Krejci D, Lozano P (2018) Space Propulsion Technology for small spacecraft. Proc IEEE 106:362–378. https://doi.org/10.1109/JPROC.2017.2778747
5. Poghosyan A, Golkar A (2017) CubeSat evolution: analyzing CubeSat capabilities for conducting science missions. Prog Aerosp Sci 88:59–83. https://doi.org/10.1016/j.paerosci.2016.11.002
6. Levchenko I, Keidar M, Cantrell J, Wu Y-L, Kuninaka H, Bazaka K, Xu S (2018) Explore space using swarms of tiny satellites. Nature 562:185–187. https://doi.org/10.1038/d41586-018-06957-2
7. Jochen Schein; Niansheng Qi (2001) Robert Binder; Mahadevan Krishnan; André Anders. *Low mass vacuum arc thruster system for station keeping missions*
8. Keidar M, Zhuang T, Shashurin A, Teel G, Chiu D, Lukas J, Haque S, Brieda L (2015) Electric propulsion for small satellites. Plasma Phys Control Fusion 57:14005. https://doi.org/10.1088/0741-3335/57/1/014005
9. Lun J Development of a vacuum arc thruster for nanosatellite propulsion 2009
10. Lev D, Myers RM, Lemmer KM, Kolbeck J, Koizumi H, Polzin K (2019) The technological and commercial expansion of electric propulsion. Acta Astronaut 159:213–227. https://doi.org/10.1016/j.actaastro.2019.03.058
11. Beilis I (2020) Vacuum Arc Ignition. Electrical breakdown. Plasma and spot phenomena in Electrical arcs. 113:143–164. https://doi.org/10.1007/978-3-030-44747-2_6
12. Kolbeck J, Anders A, Beilis II, Keidar M (2019) Micro-propulsion based on vacuum arcs. J Appl Phys 125. https://doi.org/10.1063/1.5081096
13. Filip Rysanek; John William Hartmann (2002) Jochen Schein; Robert Binder. *Microvacuum arc thruster design for a CubeSat class satellite*
14. Kramer HJ (2016) CANYVAL-X (CubeSat Astronomy by NASA and Yonsei using Virtual Telescope Alignment eXperiment). *European Space Agency [Online]*, February 25, Available online: https://www.eoportal.org/satellite-missions/canyval-x#spacecraft (accessed on 19 February 2024)
15. Kronhaus I, Schilling K, Pietzka M, Schein J (2014) Simple orbit and attitude control using Vacuum Arc Thrusters for picosatellites. J Spacecr Rockets 51:2008–2015. https://doi.org/10.2514/1.A32796
16. Polk JE, Sekerak MJ, Ziemer JK, Schein J, Qi N, Anders AA (2008) Theoretical analysis of Vacuum Arc Thruster and Vacuum Arc Ion Thruster performance. IEEE Trans Plasma Sci 36:2167–2179. https://doi.org/10.1109/TPS.2008.2004374
17. Jochen Schein; Mahadevan Krishnan; Robert Shotwell; John Ziemer. Vacuum Arc Thruster for Optical Communications Mission. In 33rd International Electric Propulsion Conference, The George Washington University, Washington DC (2013) USA, 6–10 October, ISBN 978-1-62410-098-7
18. Bai S, Wang N, Xie K, Miao L, Xia Q (2021) Performance model of vacuum arc thruster with inductive energy storage circuit. Acta Astronaut 186:426–437. https://doi.org/10.1016/j.actaastro.2021.06.008
19. Li Y-H, Pan J-Y, Herdrich G (2020) Design and demonstration of micro-scale vacuum cathode arc thruster with inductive energy storage circuit. Acta Astronaut 172:33–46. https://doi.org/10.1016/j.actaastro.2020.03.012
20. Keidar M, Schein J, Wilson K, Gerhan A, Au M, Tang B, Idzkowski L, Krishnan M, Beilis II (2005) Magnetically enhanced vacuum arc thruster. Plasma Sources Sci Technol 14:661–669. https://doi.org/10.1088/0963-0252/14/4/004
21. Aheieva K, Fuchikami S, Nakamoto M, Toyoda K, Cho M (2016) Development of a Direct Drive Vacuum Arc Thruster passively ignited for Nanosatellite. IEEE Trans Plasma Sci 44:100–106. https://doi.org/10.1109/TPS.2015.2500601

22. Chowdhury S, Kronhaus I (2020) Characterization of Vacuum Arc Thruster performance in weak magnetic nozzle. Aerospace 7:82. https://doi.org/10.3390/aerospace7060082
23. José-María (2022) Jiménez-Coronado; Johan Carvajal-Godínez. Vacuum Arc Thruster architecture for green orbit maintenance with small satellite missions. In *Space for @ll* 73rd International Astronautical Congress (IAC), Paris, France, 18–22 September; International Astronautical Congress, Ed
24. Aheieva K, Toyoda K, Cho M (2016) Vacuum Arc Thruster Development and Testing for Micro and Nano satellites. Aerosp Technol JAPAN 14:Pb91–Pb97. https://doi.org/10.2322/tastj.14.Pb_91
25. Kronhaus I, Schilling K, Jayakumar S, Kramer A, Pietzka M, Schein J (2013) Design of the UWE-4 picosatellite orbit control system using vacuum-arc-thrusters. In *33rd International Electric Propulsion Conference*, The George Washington University, Washington, D.C., USA, 6–10 October, ISBN 978-1-62410-098-7
26. Hypernova Space (2024) Hypernova Space. Available online: https://www.hypernovaspace.com/ (accessed on 8
27. Kühn M, Schein J (2022) Development of a high-reliability Vacuum Arc Thruster System. J Propul Power 38:752–758. https://doi.org/10.2514/1.B38202
28. Kühn M, Toursel C, Schein J (2021) Thrust measurements on the high efficient and Reliable Vacuum Arc Thruster (HERVAT). Appl Sci 11:2274. https://doi.org/10.3390/app11052274
29. Seranis (2023) September. Home. Available online: https://seranis.de/ (accessed on 7
30. Gadzo E, Porcelli F (2022) R Förstner; K Paetzold. Requirements Engineering Process for SeRANIS, a small satellite mission. In *DLRK 2022 Deutscher Luft- und Raumfahrtkongress* Deutscher Luft- und Raumfahrtkongress 2022; Deutsche Gesellschaft für Luft- und Raumfahrt, Ed
31. Johannes Bachmann; Artur Kinzel (2022) Francesco Porcelli; Alexander Schmidt; Andreas Knopp. SeRANIS: In-Orbit-demonstration Von Spitzentechnologie auf einem Kleinsatelliten. *Luft- Und Raumfahrt - Gemeinsam forschen und nachhaltig gestalten* DLRK Deutscher Luft- Und Raumfahrtkongress. September; Deutsche Gesellschaft für Luft- und Raumfahrt, Ed.„ Dresden, Germany, pp 27–29
32. Artur Kinzel; Johannes Bachmann (2022) Rishi Jaiswal; Manohar Karnal; Andreas Knopp. Seamless Radio Access Network for Internet of Space (SeRANIS): New Space Mission for Research, Development, and In-Orbit Demonstration of Cutting-Edge Technologies. In *Space for @ll* 73rd International Astronautical Congress (IAC), Paris, France, 18–22 September; International Astronautical Congress, Ed
33. Anders A, Brown IG, MacGill RA, Dickinson MR (1998) `Triggerless' triggering of vacuum arcs. J Phys D: Appl Phys 31:584–587. https://doi.org/10.1088/0022-3727/31/5/015
34. Teel G, Shashurin A, Fang X, Keidar M (2017) Discharge ignition in the micro-cathode arc thruster. J Appl Phys 121. https://doi.org/10.1063/1.4974004
35. Schein J, Qi N, Binder R, Krishnan M, Ziemer JK, Polk JE, Anders A (2002) Inductive energy storage driven vacuum arc thruster. Rev Sci Instrum 73:925–927. https://doi.org/10.1063/1.1428784

Publisher's Note